ARL-TR-10217 ● SEP 2025

DEVCOM ARMY RESEARCH LABORATORY

A System of Aqueous Electrolyte Gels Exhibiting Double Glass Transitions and High Conductivities

by Michael S. Ding, Arthur V. Cresce, and Patricia M. Gonzales

NOTICES

Disclaimers

The findings in this report are not to be construed as an official Department of the Army position unless so designated by other authorized documents.

Citation of manufacturer's or trade names does not constitute an official endorsement or approval of the use thereof.

Destroy this report when it is no longer needed. Do not return it to the originator.

ARL-TR-10217 ● SEP 2025

A System of Aqueous Electrolyte Gels Exhibiting Double Glass Transitions and High Conductivities

Michael S. Ding and Arthur V. Cresce
DEVCOM Army Research Laboratory

Patricia M. Gonzales
University of Maryland

REPORT DOCUMENTATION PAGE

1. REPORT DATE	2. REPORT TYPE	3. DATES COVERED	
		START DATE	END DATE
September 2025	Technical Report	1 October 2023	30 September 2024

4. TITLE AND SUBTITLE
A System of Aqueous Electrolyte Gels Exhibiting Double Glass Transitions and High Conductivities

5a. CONTRACT NUMBER	5b. GRANT NUMBER	5c. PROGRAM ELEMENT NUMBER
W911NF-22-2-0021		
5d. PROJECT NUMBER	**5e. TASK NUMBER**	**5f. WORK UNIT NUMBER**

6. AUTHOR(S)
Michael S. Ding, Arthur V. Cresce, and Patricia M. Gonzales

7. PERFORMING ORGANIZATION NAME(S) AND ADDRESS(ES)
DEVCOM Army Research Laboratory
ATTN: FCDD-RLA-GD
Adelphi, MD 20783-1138

8. PERFORMING ORGANIZATION REPORT NUMBER
ARL-TR-10217

9. SPONSORING/MONITORING AGENCY NAME(S) AND ADDRESS(ES)	10. SPONSOR/MONITOR'S ACRONYM(S)	11. SPONSOR/MONITOR'S REPORT NUMBER(S)

12. DISTRIBUTION/AVAILABILITY STATEMENT
DISTRIBUTION STATEMENT A. Approved for public release: distribution unlimited.

13. SUPPLEMENTARY NOTES
ORCIDs: Michael S. Ding, 0000-0002-9302-1032; Arthur V. Cresce, 0000-0002-3894-6083; Patricia M. Gonzales, 0000-0002-2318-1591

14. ABSTRACT
We characterized and studied a system of polymer-supported aqueous electrolytes containing a series of gels that exhibited double glass transitions and high conductivities. These electrolytes, composed of a 12-m aqueous solution of lithium bis(trifluoromethanesulfonyl)imide and a monomer of poly(ethylene glycol) diacrylate (PDA), were characterized, both before and after polymerization by ultraviolet irradiation, with thermoconductometry, rheometry, and glass transition analysis. For the gel compositions, the polymerization transformed the starting solution of a single liquid structure into the gel of a polymer-solution double substructure, as evidenced by the emergence of a double glass transition in these gels. Individually, the polymer substructure in the gel gave it a storage modulus that rose rapidly with its PDA content, and the solution substructure, an unusually high conductivity. The generation of a polymer substructure in a gel also made the remaining solution substructure more conductive and less viscous, resulting in conductivity gains upon polymerization and in other unusual phenomena. The coexistence in the gel of two substructures, separately responsible for its mechanical and electrical properties and amenable to alterations in chemical composition and materials processing, holds great interest and promise for future electrolyte development.

15. SUBJECT TERMS
Energy Sciences, aqueous electrolytes, gels, polymerization, glass transition, conductivity, storage modulus

16. SECURITY CLASSIFICATION OF:			17. LIMITATION OF ABSTRACT	18. NUMBER OF PAGES
a. REPORT	b. ABSTRACT	C. THIS PAGE		
UNCLASSIFIED	UNCLASSIFIED	UNCLASSIFIED	UU	31

19a. NAME OF RESPONSIBLE PERSON	19b. PHONE NUMBER *(Include area code)*
Michael S. Ding	(520) 691-4895

STANDARD FORM 298 (REV. 5/2020)
Prescribed by ANSI Std. Z39.18

Contents

List of Figures

1. Introduction

This work characterizes and studies a system of polymer-supported aqueous electrolytes containing a series of gels that exhibit double glass transitions, unusually high conductivities, and other interesting properties, following a pioneering study on a different system of the same type of electrolytes.[1,2] The present system was made of, as starting materials, two fully miscible components of a 12-m aqueous solution of lithium bis(trifluoromethanesulfonyl)imide (LiTFSI) and a liquid of poly(ethylene glycol) diacrylate of Mn 575 monomer (PDA for short in this report), which we will denote as wPDA + (1–w)LiTFSI$_{12m}$H$_2$O with w in mass fraction. Polymerization of such a starting material with UV irradiation turned it into a gel, a solid, or another liquid, depending on the value of w. The sample compositions covered the entire w range, and were selectively characterized by the techniques of thermoconductometry,[3] glass transition analysis,[2] and rheometry,[4,5] both before and after the UV irradiation of the samples. Structurally, the irradiation polymerized the PDA monomers in the starting composition and generated in it a polymer network substructure and a solution substructure, the two being mutually soluble but distinct from each other in their manifestations in the properties of the irradiated material. One such manifestation was the transformation of the single glass transition of a starting liquid into a double glass transition in the polymerized gel. Another was the rapid rise in the storage modulus of the gel with its w due solely to the polymer substructure. Still another manifestation of crucial importance was the unusually high conductivities of these gels despite their high rigidity, which was attributed to the existence of the solution substructure. This coexistence of two substructures in a single homogeneous body, separately responsible for the mechanical and electrical properties of the body, amenable to alterations in chemical composition and materials processing, seems to hold great importance and promise for future electrolyte development; this work therefore has been focused on the study of the electrical, thermal, and mechanical properties in relation to material structure of this type of materials using PDA + LiTFSI$_{12m}$H$_2$O as the model material.

Interest in polymer and gel electrolytes for batteries has been with us since the beginning of the lithium-ion battery research and development,[6–14] where the gel electrolyte differs from the polymer electrolyte in having an immobilized solution dissolved in a polymer network.[15] The dissolved solution, by forming liquid channels for ion transfer, can readily support an ionic current, thus making a gel electrolyte substantially more conductive than a polymer electrolyte, which rely on either polymer segmental motion or interchain hopping for ion conduction.[16–19] Meanwhile, by having an internal polymer framework, the gel electrolyte retains

many of the advantages of a true polymer: a degree of mechanical integrity, the absence of a liquid phase, reduced reactivity and flammability, and enhanced engineering possibilities for the devices in which such an electrolyte is used.

2. Methods

2.1 Sample Preparation

A LiTFSI salt purchased from Gotion was mixed with distilled water to the concentration of 12 molality to form the host solution of $LiTFSI_{12m}H_2O$ for the subsequent additions of PDA (Mn 575) monomer purchased from Sigma-Aldrich. The sample compositions so prepared followed the green dotted line in the composition triangle of LiTFSI, H_2O, and PDA of Figure 1. Polymerization of these compositions was via UV irradiation with a UV oven, Intelliray 600 by Uvitron International, at the typical settings of 100% power (600 W) at a lamp-sample distance of 5 cm and 180-s duration.[1,20] The initiator for the polymerization was 2-hydroxy-2-methylpropiophenone by Sigma-Aldrich, which was added in the amount of about 1 to 2 wt% of the PDA in the sample.

For efficiency of experimentation and to focus on the effects of polymerization of a material on its properties, the thermoconductometric measurements on the wPDA + $(1–w)LiTFSI_{12m}H_2O$ samples of $w \leq 0.42$ were conducted in pairs: a complete measurement on a pre-UV liquid, followed by the addition of the initiator and an in-situ UV irradiation, and then followed by another complete measurement on the post-UV sample, which now could be a liquid, a gel, or a solid depending on the value of w. The glass transition analysis was performed on every composition, both pre- and post-UV. Rheometric measurement was done only on the post-UV compositions that formed a gel. The selective application of the different characterization techniques to different groupings of compositions is indicated by the legends of Figure 1.

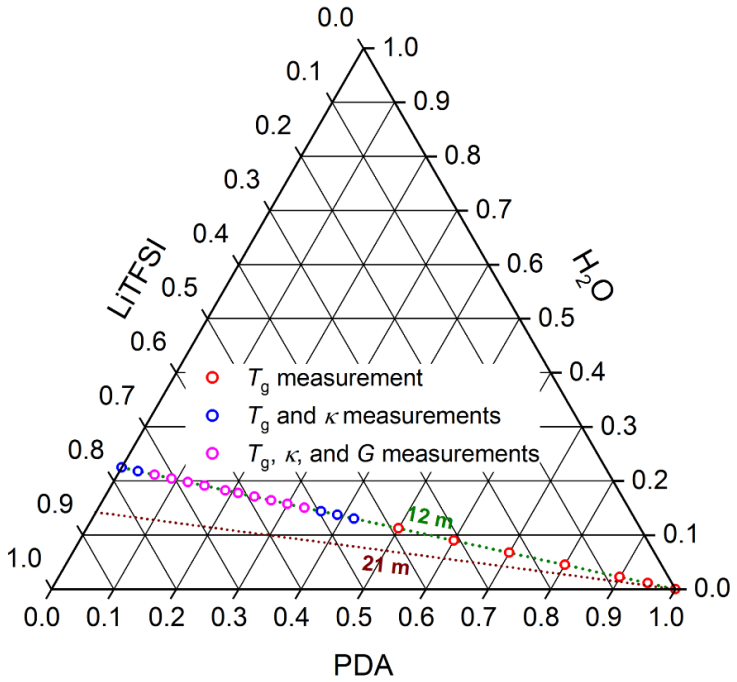

Figure 1. The chemical compositions in mass fraction, *w*, of the polymer-supported aqueous electrolytes of the system *w*PDA + (1–w)LiTFSI$_{12m}$H$_2$O containing the gels that exhibited double glass transitions and high conductivities. On these compositions, thermoconductometric (κ), glass transition (T_g), and rheometric (G) studies were selectively conducted as appropriate, as indicated by the legends. The green arrow indicates the direction of increasing *w* in the way the samples were prepared and measured. The brown dotted line depicts the compositions in a *w*PDA + (1–w)LiTFSI$_{21m}$H$_2$O system studied in a previous work and plotted here for comparison.

2.2 Differential Scanning Calorimetry (DSC) Analysis of Glass Transitions

The thermal signal of a glass transition in a sample was measured and analyzed using a commercial differential scanning calorimeter (Discovery DSC 250 by TA Instruments) with a liquid nitrogen cooler for low-temperature control and a calibration with the standards of cyclohexane (–87.06 °C for a solid-solid transition and 6.45 °C for melting) and indium (156.60 °C for melting). The sample was prepared by hermetically enclosing about 10 mg of a sample material in a pair of aluminum pan and lid (0219-0062 and 0219-0061 by PerkinElmer Instruments). This sample was then rapidly cooled by the DSC at its fastest rate of about 50 °C/min to vitrify the sample and subsequently heated up uniformly at 5 °C/min for the determination of its glass transition. This heating rate seemed to offer the best compromise between the signal strength (higher rate) and temperature resolution (lower rate) based on a limited number of tests at different heating rates on different sample compositions.

2.3 Rheometric Determination of Storage Modulus of Gels

The storage modulus of a gel sample was determined on a commercial rheometer, model AR-G2 by TA Instruments, operated in its oscillatory mode. The sample was made into a disc 25.4 mm in diameter and about 2 mm thick, which was placed onto the rheometer between a circular plate geometry of 25.4-mm diameter and a Peltier bottom plate that had been kept at 25 °C. To prevent slipping, the measuring thickness of the sample was adjusted before a measurement by raising or lowering the geometry to ensure that a moderate normal force was applied to the sample disc, which was typically around 1–2 N depending on the sample composition, and was insensitive to the measurement results. The measurement frequency was scanned from 0.1 to 100 Hz, and the measurement strain was kept at around 1%, the level of which had been determined to be within the viscoelastic region prior to the measurement. Finally, the value at 1 Hz from each scan was collected for the modulus value of these gel materials.[4,5]

2.4 Thermoconductometric Measurement

The sample-holding cell was made of two nickel rods for the conductivity electrodes, adapted from a commercial conductivity cell YSI 3418 and a polypropylene bottle for the cell body, which was largely transparent to the UV irradiation. Each of the two electrodes was tightly wrapped on the upper part in a shrink tube to fix the effective cell constant. These electrodes were attached to the screw cap of the polypropylene bottle with a hermetic fit, and the complete sample cell was calibrated with a KCl standard solution for its cell constant.

For a thermoconductometric run, the sample was first cooled from 50 to –60 °C at a slow rate of 0.1 °C/min and then heated back up at the same rate within a PC-controlled Tenney Jr. Engineering Environmental Chamber. Meanwhile, the temperature of the sample bottle, along with that of a reference positioned nearby, was recorded with two digital thermometers via two T-type thermocouples, one attached to the sample bottle and the other the reference, at a rate of 320 readings/min for each channel. The reference was of the same kind as the sample bottle but contained propylene carbonate as the reference material, which had been tested to remain in the liquid state without any phase change in the entire testing regime.

Simultaneously, the impedance of the sample was recorded using a Keysight E4980A Precision LCR Meter, with continuously repeating frequency scans from 20 Hz to 2 MHz at a constant voltage amplitude of 200 mV, each scan consisting of 150 readings. After the completion of the thermoconductometric run, a conductivity value was calculated from each of the impedance scans on the Nyquist

plot of the 150-point impedance curve at the intersection of this curve with the real axis, which was paired with a sample temperature and a temperature differential taken at the time this intersection occurred. This led to an effective sampling rate of about 1.1 points/min for the conductivity measurement.[1]

3. Results and Discussion

3.1 Double Glass Transitions and Their Extrapolation to Determine the Gel Range

The glass transition of a component in a material is an event when the internal molecular motion in the component starts to lag the rate of the external cooling to which the material has been subjected.[21] As such, the determination of this glass transition temperature, θ_g (θ_g / °C = T_g / K – 273.15), can be used to detect the existence of the component and, when multiple types of components with sufficiently different internal molecular mobilities are present, multiple θ_g's can be determined with higher and lower temperatures pointing to less and more mobile components, respectively. Furthermore, the relative strength of the thermal signal from which a θ_g is determined indicates the abundance of the associated component.

When a PDA + LiTFSI + H_2O solution is polymerized into a gel, the single liquid structure of the solution is differentiated into two substructures: the newly generated polymer substructure and the remaining solution substructure, mutually soluble yet distinct from each other. Such a gel should yield, under the right conditions, a double glass transition with two distinct glass transition temperatures, $\theta_{g,p}$ and $\theta_{g,s}$, corresponding to the polymer and solution substructures. Such a double glass transition was first observed in a previous work on the gels of PDA + $LiTFSI_{21m}H_2O$ in the form of a protracted transition step in the DSC heat flow curve enveloping two glass transitions. There, the relative weakness of the double transition signals and their proximity in temperature necessitated some extrapolation for the resolution of the $\theta_{g,p}$-$\theta_{g,s}$ pairs.[2] In contrast, the gels in the present wPDA + (1–w)$LiTFSI_{12m}H_2O$ system displayed much more distinct thermal signals for their $\theta_{g,p}$–$\theta_{g,s}$ pairs, as shown in Figure 2a by the DSC heat flow curves, from which the $\theta_{g,p}$ and $\theta_{g,s}$ could now be evaluated without the need of extrapolation. These $\theta_{g,p}$ and $\theta_{g,s}$ values form two distinct tracks and, if plotted against the w values as marked on the plot, would reveal their individual dependencies on the w.

Another set of important dependencies emerges when the height of the glass transition steps in heat flow is plotted against w, as shown in Figure 2a. With a

rising w, this height increases on the $\theta_{g,p}$ track and decreases on the $\theta_{g,s}$ track, reflecting the rising and falling abundances of the polymer and solution substructures, respectively. As the heat flow in DSC is proportional to the heat capacity, C_p, of the sample,[22] the height of a glass transition step corresponds to the change in C_p at the glass transition. This change of ΔC_p was calculated from the heat flow curves of Figure 2a and plotted against w in Figure 2b as $\Delta C_{p,p}$ and $\Delta C_{p,s}$ for the polymer and solution substructures. These points of $\Delta C_{p,p}$ and $\Delta C_{p,s}$ can be linearly extrapolated to the x-axis where $\Delta C_p = 0$, as is done in Figure 2b with the red and blue lines. The composition at the interception of the x-axis with the extrapolated red line signifies the lower limit of the gel range where $\Delta C_{p,p}$ starts to appear with increasing w, while that with the extrapolated blue line signifies the upper limit where $\Delta C_{p,s}$ disappears. As this method of finding the limits of the gel range relies on measured data in a statistical way and is continuous in the evaluation of these limits, it should be more reliable and accurate than those relying on a set of limited and discreet compositions. The gel range of (0.045, 0.31) so evaluated triples that of the PDA + LiTFSI$_{21m}$H$_2$O system determined in a previous study,[2] as marked respectively by the black and gray dotted lines in Figure 2b. This tripling of gel range seems to result from the richer H$_2$O content (an increase of 58 wt%) in the present system, which demonstrates an added advantage of using 12 m instead of the previous 21-m LiTFSI + H$_2$O solution, and to inform the importance of the hydrogen bonding in the formation of the polymer substructure in these gels.

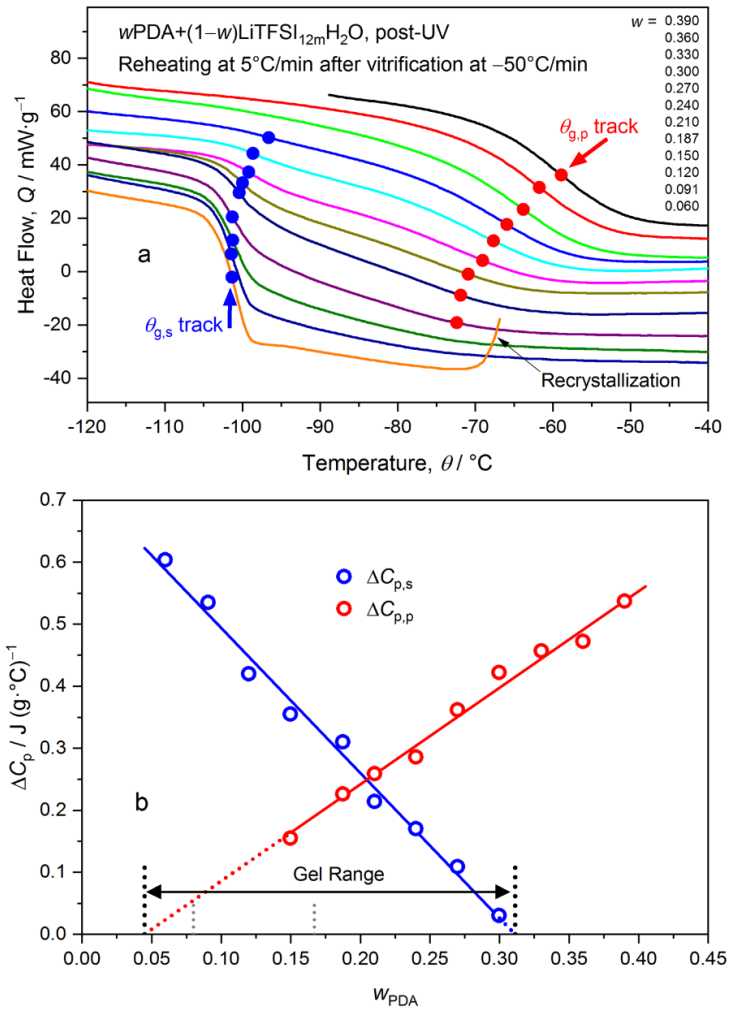

Figure 2. **(a) DSC heat flow curves of post-UV *w*PDA + (1–*w*)LiTFSI$_{12m}$H$_2$O electrolytes with the *w* values encompassing those for which a double glass transition was observed, to demonstrate the existence of two distinct tracks of glass transition temperature, $\theta_{g,s}$ and $\theta_{g,p}$, as marked with the blue and red dots. For visual clarity, the curves have been shifted in the vertical direction without affecting either the θ_g values or the changes in the heat flow curves. The sharp rise on the curve of *w* = 0.06 sample after glass transition signals the onset of a recrystallization from the supercooled liquid sample. (b) The height of the glass transition steps in the form of ΔC_p vs. *w* corresponding to the blue and red dots in (a). As illustrated in the plot, the associated linear trend lines are extrapolated to $\Delta C_p = 0$ to obtain the gel range of the present system as marked by the two dotted black lines, with that of a previously studied system of PDA + LiTFSI$_{21m}$H$_2$O marked by the two dotted gray lines for comparison.**

3.2 Dependency of Glass Transition Temperatures on PDA Content and Polymerization

For a more comprehensive view of the changes in θ_g's with *w* and with polymerization, including those shown in Figure 2, Figure 3 plots all the θ_g's versus *w* for all the compositions prepared in this study, both pre- and post-UV, against the backdrop of the physical states of the post-UV materials as determined by the

ΔC_p extrapolation just described, the rheological investigation to be presented next, and some additional direct observations. As can be seen, the pre-UV wPDA + (1–w)LiTFSI$_{12m}$H$_2$O electrolytes, being all in the liquid state with a single glass transition, exhibit θ_g's forming a single curve connecting the θ_g of the LiTFSI$_{12m}$H$_2$O solution to that of the PDA with a hill in the middle peaking at about $w = 0.75$. This hill is likely the result of attractive intermolecular interactions among the molecules of H$_2$O and PDA and the ions of Li^+ and $TFSI^-$ leading to a dynamic network and an increase in the viscosity of the liquid.

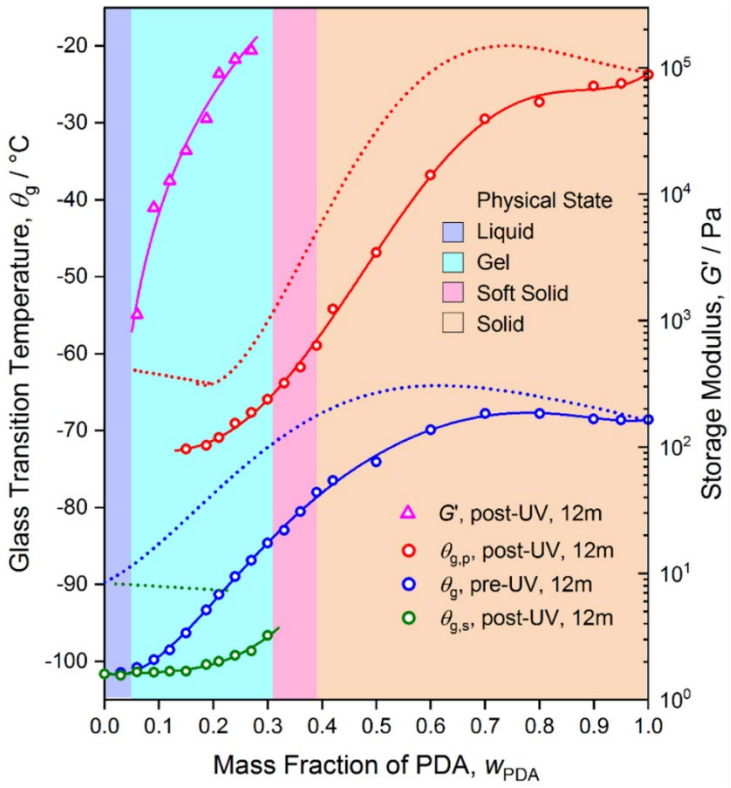

Figure 3. Glass transition temperatures, θ_g, and storage modulus, G', as functions of mass fraction of PDA, w, in wPDA + (1–w)LiTFSI$_{12m}$H$_2$O electrolytes. The blue dots (θ_g) represent the glass transition temperatures of the pre-UV liquids, and the green ($\theta_{g,s}$) and red ($\theta_{g,p}$) dots plot those of the solution and polymer substructures, respectively, in the post-UV electrolytes. For comparison, the dotted curves are from a previous system of PDA + LiTFSI$_{21m}$H$_2$O, associated by color with their counterparts in the present system.

For the post-UV electrolytes, there are two tracks of glass transition temperatures, $\theta_{g,s}$ and $\theta_{g,p}$, corresponding to the solution and polymer substructures, as plotted in Figure 3 with the green and red dots, respectively. As w increases from 0, the $\theta_{g,s}$ track starts out at the θ_g value of the LiTFSI$_{12m}$H$_2$O solution, remains flat to about $w = 0.17$, then rises slightly, all the while growing weaker in signal strength and eventually fading out at about $w = 0.31$. Meanwhile, the $\theta_{g,p}$ track emerges at $w = 0.15$, about 30 °C above the $\theta_{g,s}$ track due to the much lower molecular mobility of the polymer substructure, grows in strength and rises up in value, and then

becomes a single track beyond $w > 0.31$, which subsequently follows a trajectory largely in parallel to that of the blue dots, likely with the same underlying molecular mechanisms. As to the effect of polymerization, it is worth noticing that the $\theta_{g,s}$ of the post-UV electrolytes deviate from the $\theta_{g,}$ of their precursors toward low temperature, indicating a progressive reduction in the viscosity of the solution substructure. This is likely the result of the polymerization linking together the PDA monomers, extricating them from the PDA + $LiTFSI_{12m}H_2O$ mixture and effectively "purifying" it.

At a glance, the θ_g, $\theta_{g,s}$, and $\theta_{g,p}$ lines of the present system behave similarly to their counterparts in the previous PDA + $LiTFSI_{21m}H_2O$ system plotted with the dotted lines in Figure 3, apart from their downward tilts toward the $w = 0$ axis due to the lower value of θ_g of the $LiTFSI_{12m}H_2O$ solution than of the $LiTFSI_{21m}H_2O$ (by about 11 °C). Upon closer inspection, the present system possesses a wider range in which both $\theta_{g,s}$ and $\theta_{g,p}$ were measurable, and a greater separation between the $\theta_{g,s}$ and $\theta_{g,p}$ curves, which, together with the stronger thermal signals for these $\theta_{g,s}$–$\theta_{g,p}$ pairs, enabled a more definitive and accurate measurement of these $\theta_{g,s}$–$\theta_{g,p}$ pairs and an extrapolative determination of its gel range with better accuracy and precision.

3.3 Rapid Rise of Storage Modulus with the PDA Content in the Gels

When the storage moduli, G', of the gels in the wPDA + (1–w)$LiTFSI_{12m}H_2O$ system were determined using a rheometer in its oscillatory mode and plotted against w, they rise quickly with w, as shown in Figure 3 with the pink triangles, particularly in the more dilute part of the gel range. When viewed in conjunction with the w-dependencies of $\theta_{g,s}$ and $\theta_{g,p}$ of these materials, it can be discerned that in the more dilute part of the gel range before the emergence of the $\theta_{g,p}$ track ($w < 0.15$), there is little correlation between the rapid rise of G' and the near constancy of $\theta_{g,s}$. It follows that the rapid rise in G' had to be due to the strengthening of the polymer substructure even though its $\theta_{g,p}$ was yet to be measurable at these low w values. When the $\theta_{g,p}$ eventually emerges at $w = 0.15$, it is 30 °C above in value, pointing to a much more viscous polymer substructure, and it then trends upward more rapidly than the $\theta_{g,s}$, consistent with the polymer substructure being solely responsible for the rigidity of the gel electrolyte materials.

3.4 Conductivities of the Electrolytes Before and After Polymerization

While the polymer substructure in a gel was responsible for the rapid rise of its storage modulus with w, as has just been shown, the solution substructure gave rise

to its unusually high conductivity as we present here. This conductivity was experimentally determined in this study by using our thermoconductometry,[1,3] of which a typical run yields a pair of synchronized curves of conductivity, κ, and temperature differential, $\Delta\theta$. On the κ curve, the values of the first cooling segment without any precipitation or other phase change were used to represent the true values of the electrolyte. This procedure was repeated for every composition of the *w*PDA + (1–*w*)LiTFSI$_{12m}$H$_2$O system with *w* values ranging from 0 to 0.42, generating two sets of experimental κ values in the space of θ and *w*, one set for the pre-UV samples and one for post-UV. These sets were then each fitted with a parameterized Vogel−Fulcher−Tammann (VFT) function to produce two $\kappa(\theta, \mathrm{w})$ functions.[23] For the pre-UV materials, the fitting yielded

$$\ln \kappa_{\text{pre-UV}} = 10.7151 - 2.22907w + 9.95038w^2 - (748.809 + 2222.06w^2)/(137.762 - 107.024w + 144.577w^2 + \theta) - 0.5\ln(273.15 + \theta)\,, \quad (1)$$

where κ is in the units of mS·cm^{-1} and the average fitting error was 0.27% of the data range. Equation 1 is plotted in Figure 4 both as $\kappa(\theta)$ curves (Figure 4a) with the measured data points to show the closeness of the fit and as a $\kappa(\theta, w)$ surface (Figure 4b) to show the simultaneous changes of κ with θ and *w*.

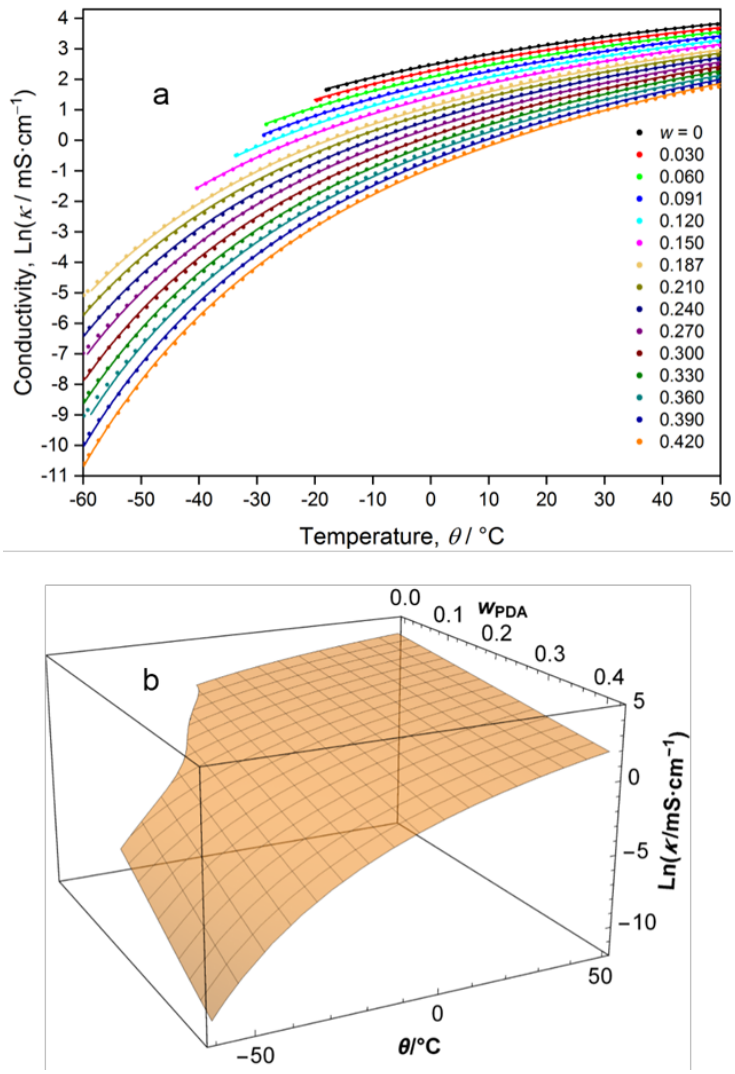

Figure 4. Electrolytic conductivity κ of the pre-UV samples of wPDA + (1–w)LiTFSI$_{12m}$H$_2$O of w mass fraction, plotted against temperature θ as curves in (a) with their w values indicated, and against (θ, w) as a surface in (b). In (a), the dots represent the measured data and the solid lines plot their fitting function of Equation 1 at the indicated w values, while in (b) the surface plots Equation 1 in its entirety within the boundaries outside in which an electrolyte became nonhomogeneous because of the precipitation of a second phase.

For the sample materials after the UV irradiation,

$$\ln \kappa_{\text{post-UV}} = 10.429 + 22.0098w^3 - (670.762 + 757.854w + 12527.4w^3 - 15376.7w^4)/(129.963 - 62.0312w^2 + \theta) - 0.5\ln(273.15 + \theta)\,, \quad (2)$$

where κ is in the units of mS·cm^{-1} and the average fitting error was 0.39% of the data range. Equation 2 is plotted in Figure 5 as both $\kappa(\theta)$ curves (Figure 5a) and a $\kappa(\theta, w)$ surface (Figure 5b) for post-UV materials. From Figures 4 and 5, one can see that the $\kappa(\theta, w)$ surfaces of the pre- and post-UV electrolytes are similarly shaped, with κ falling steadily with both a rising w and a falling θ.

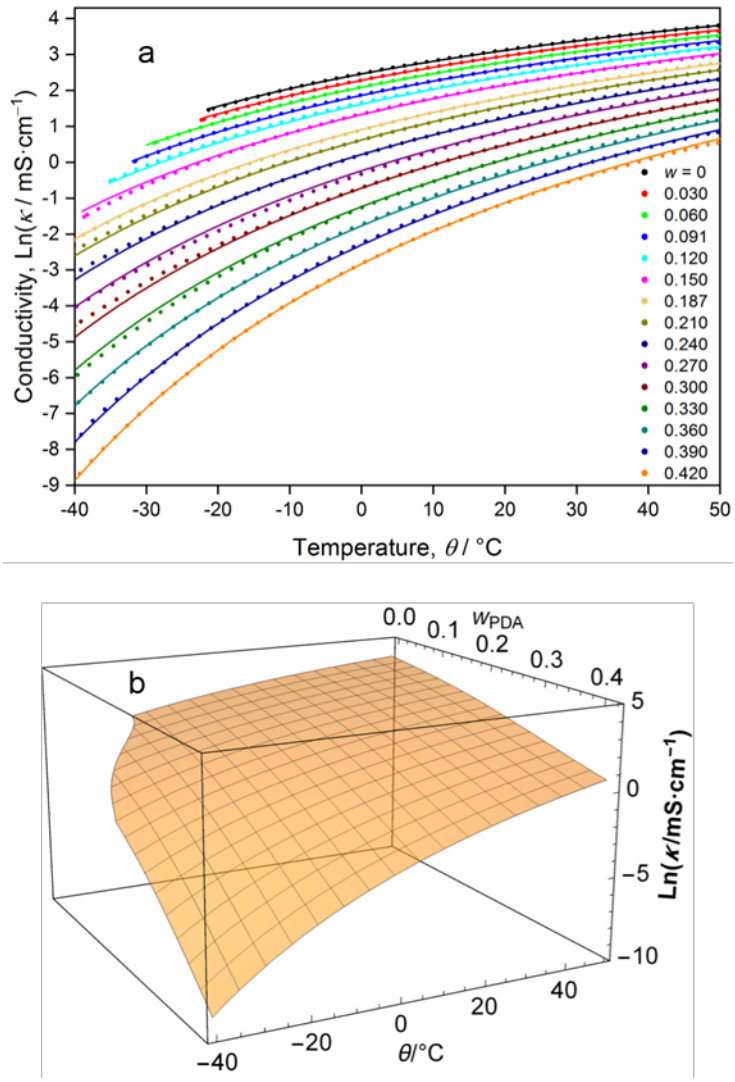

Figure 5. Electrolytic conductivity κ of the post-UV samples of wPDA + (1–w)LiTFSI$_{12m}$H$_2$O of w mass fraction, plotted against temperature θ as curves in (a) with their w values indicated, and against (θ, w) as a surface in (b). In (a), the dots represent the measured data and the solid lines plot their fitting function of Equation 2 at the indicated w values, while in (b) the surface plots Equation 2 in its entirety within the boundaries outside of which an electrolyte became nonhomogeneous because of the precipitation of a second phase.

3.5 Conductivity Gain upon Polymerization as a Function of PDA Content and Temperature

To observe the effects of polymerization on conductivity more clearly and precisely, we derive from Equations 1 and 2 a new function g_κ, the conductivity gain upon polymerization:

$$g_\kappa \equiv \left(\kappa_{\text{post-UV}}/\kappa_{\text{pre-UV}} - 1\right) \times 100\% \,. \tag{3}$$

Equation 3 is plotted in Figure 6 as both a surface (Figure 6a) and a contour plot (Figure 6b). It is striking to see that in a considerable area near the corner of low w and θ, mostly contained in the gel area (the red rectangle), the act of polymerization raised the κ of the polymerized electrolytes above their precursors, as reflected by the positive values in g_κ. This is likely the result of the polymerization extricating the PDA monomers from being mixed with the $LiTFSI_{12m}H_2O$ solution in a precursor, thus raising the conductivity of the solution to such an extent as to offset the resistance put up by the newly created polymer substructure. Even when g_κ is negative, the conductivity decline by polymerization is quite limited in the rest of the gel area drawn in Figure 6. That an electrolyte of a gel composition exhibits, upon polymerization, a sizeable rise or a limited fall in κ, while experiencing a dramatic increase in rigidity, is a direct consequence of the coexistence of the polymer and solution substructures, separately giving rise to the desirable mechanical and electrical properties, respectively. The same behavior has been observed in the previous PDA + $LiTFSI_{21m}H_2O$ system.[2]

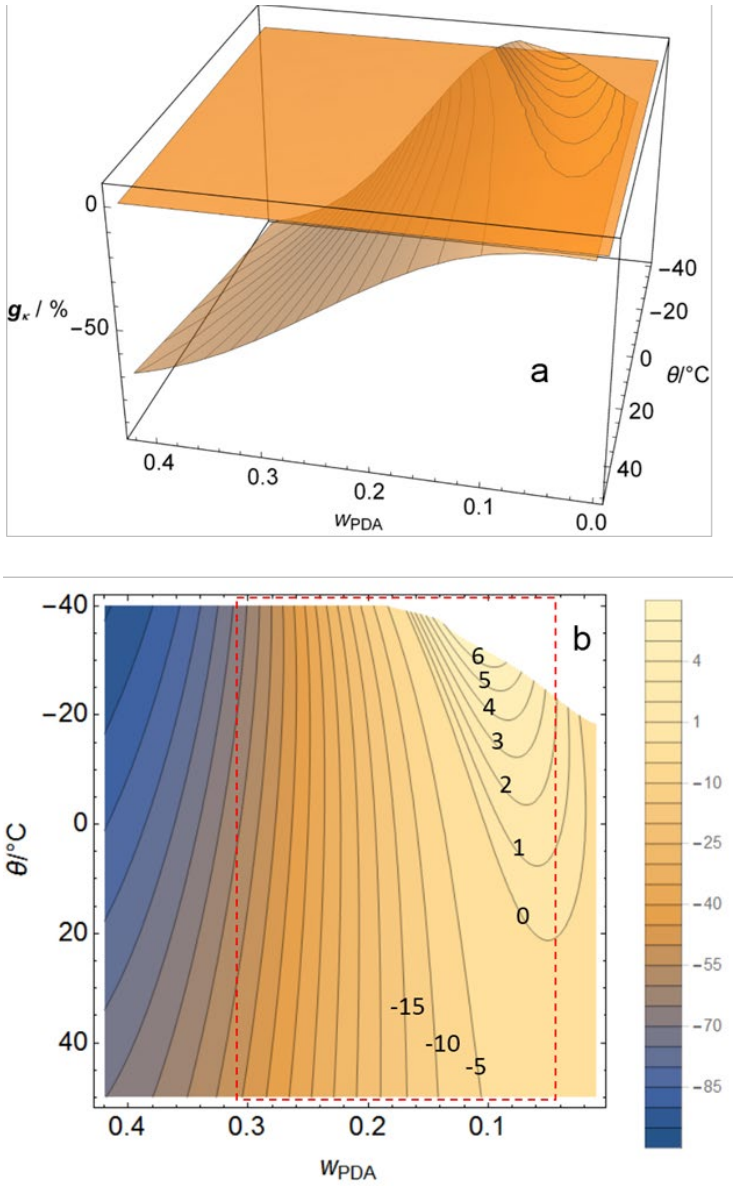

Figure 6. Conductivity gain upon polymerization, g_κ, as defined by Equation 3, plotted as a surface (a) and a contour plot (b) in the coordinates of temperature, θ, and mass fraction, w, for wPDA + (1–w)LiTFSI$_{12m}$H$_2$O electrolytes. The contour lines are of the interval of 5% below 0% and 1% above, with the zero-line delineated by the intersection of the g_κ surface with the zero plane in (a) and marked with 0 in (b). The red rectangle in (b) is an overlay of the (w, θ)–boundaries for the gel compositions. A part near the corner of low w and θ is missing because of the precipitation of a second phase during the measurements.

3.6 High Conductivities of the Gels as Compared to Several Other Types of Electrolytes

To demonstrate the unusually high conductivities of the gels in the present system, Figure 7 plots the conductivity values of a representative gel of 0.18 PDA + 0.82 LiTFSI$_{12m}$H$_2$O against a few other electrolytes. First, it is more than 2 orders of

magnitude more conductive than the two polymer electrolytes of 188 mol% LiFSI + PEC and $(PEO)_{10}$LiTFSI, chosen for their best conductivities in their respective classes.[24] This is because the present gel was able to retain a distinct and connected solution substructure for the conduction of ions as opposed to the true polymer electrolytes relying on segmental motion and ion-hopping for the ion transfer. Second, at room temperature and above, it is more conductive than even some widely used liquid electrolytes of carbonate solvents, each chosen for its high κ values in its class.[3,25,26] Finally, it is considerably more conductive than the other gel of the same type from a previous study, of the composition 0.12 PDA + 0.88 $LiTFSI_{21m}H_2O$, primarily due to the considerably higher conductivities of the $LiTFSI_{12m}H_2O$ solution than those of $LiTFSI_{21m}H_2O$.[1,23]

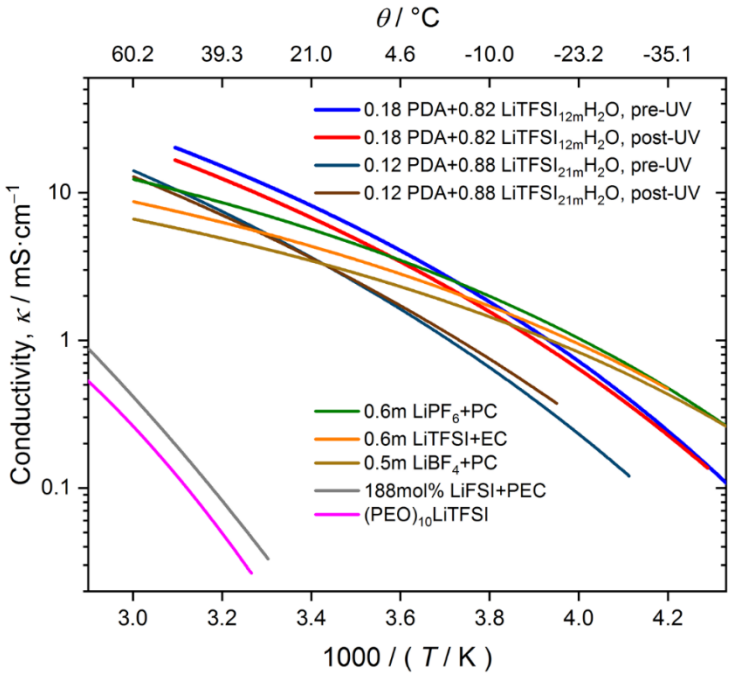

Figure 7. Exceptional conductivities of PDA + $LiTFSI_{12m}H_2O$ gels, as typified by those of the 0.18PDA + 0.82$LiTFSI_{12m}H_2O$ gel plotted here in red, in comparison to the best values of two typical true polymer electrolytes, 188 mol% LiFSI + PEC and $(PEO)_{10}$LiTFSI, of some common liquid electrolytes of carbonate solvents, and of a gel electrolyte of the same type with a more concentrated solution, as identified by the legends.

3.7 Vanishing Conductivity Temperatures and Their Inversion Upon Polymerization

Another characteristic of the electrolyte related to their conductivity, the vanishing conductivity temperature, T_0, was obtained by fitting the measured $\kappa(\theta)$ data at discreet values of w with the VFT equation

$$\kappa = \mathrm{A}\exp\left(-\frac{E_a}{R}\frac{1}{T-T_0}\right), \qquad (4)$$

where A, E_a, R, and T are pre-exponential factor, activation energy, gas constant, and temperature in kelvin, respectively.[27] As Equation 4 indicates, κ vanishes when T reaches T_0, hence its name.[28] As plotted in Figure 8 with the blue and green triangles, the fitting results of θ_0 (θ_0 / °C = T_0 / K – 273.15) for the post-UV samples are consistently and significantly below those of their pre-UV counterparts, leading to the counterintuitive result that a semi-solid gel would cease to conduct ions at a lower temperature than a true liquid of the same overall composition. This is mainly a consequence of the lower viscosity of the "purer" solution substructure becoming increasingly more dominant in determining the ionic conductivity at lower temperatures.

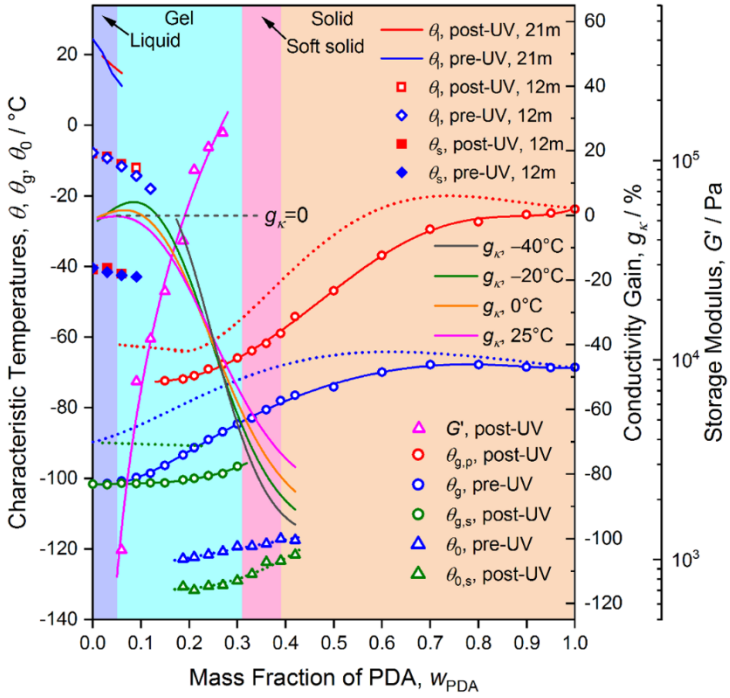

Figure 8. Liquidus and solidus temperatures, θ_l and θ_s, glass transition temperatures, θ_g, $\theta_{g,p}$, and $\theta_{g,s}$, vanishing conductivity temperatures, θ_0 and $\theta_{0,s}$, and conductivity gains, g_κ, as functions of mass fraction of PDA, w, of the wPDA + (1−w)LiTFSI$_{12m}$H$_2$O electrolytes, plotted together against the backdrop of physical states of the polymerized electrolytes, to demonstrate the dependencies of these properties on w and the correlations among them with respect to w and to polymerization.

3.8 Lowering of Liquidus Temperatures with PDA Content

One more crucial characteristic of an electrolyte material is the temperature range in which it is thermodynamically stable against the precipitation of a component. This range is thus limited on the lower end by the liquidus point, θ_l, for a liquid electrolyte, or a gel electrolyte by extension. Experimentally, the θ_l was determined here by locating on the $\Delta\theta$ curve of a thermoconductometric scan the endset point of the liquidus melting event. The results are plotted in Figure 8 for the present

(open diamonds and squares) and previous (solid blue and red lines) systems.[1] Comparison of these two sets of θ_l data shows that by using 12-m aqueous solution instead of 21 m, the thermodynamic stabilities of the resulting gels have been expended more than 30 °C into the lower temperatures.

Another important feature to point out on these θ_l lines in Figure 8 is the steady fall of the θ_l points with the PDA content, which is attributable to the entropic effect of freezing point depression by the addition of PDA molecules into an $LiTFSI_mH_2O$ solution and the enthalpic effect of molecular affinity between these two components.[29,30] As for the effects of polymerization on these θ_l lines, we see that the falls with w are reduced by the polymerization, which can be explained both entropically and enthalpically. Entropically, the polymerization reduces the number of PDA particles and thus lessens the freezing point depression. Enthalpically, it enlarges the PDA molecules, which would likely reduce their affinity with the $LiTFSI_mH_2O$ solution due to the reduced ability of their subunits to form hydrogen and electrostatic bonds with the H_2O and the ions in the solution.

3.9 Putting It All Together: Broader Connections Among the Various Properties

To see the broader connections among all the various properties measured, determined, or calculated for the wPDA + $(1-w)LiTFSI_{12m}H_2O$ materials in this study, they are plotted together versus w against the backdrop of the physical states of these materials in Figure 8. As shown in the figure, most of the properties measured, or measurable, are in the w-range extending from 0 to a little over the upper limit of the gel range. Also in the same range, the properties change the most and do so in the most interesting ways. These changes can be consistently explained based on the existence of the polymer and solution substructures in the post-UV materials and the shifting balance of dominance of these substructures, from the total dominance by the solution substructure in the liquid region, through their co-dominance in the gel region, to the total dominance by the polymer substructure in the solid region.

This shifting of dominance is most strikingly reflected in the w dependency of the glass transition temperatures of the post-UV electrolytes. In the liquid region with low w's, there is little polymer substructure created by the UV irradiation, and the $\theta_{g,s}$ of the post-UV materials is essentially constant, equaling the value of $LiTFSI_{12m}H_2O$, as it is dictated solely by the solution substructure. As w enters the gel region, the $\theta_{g,s}$ starts to deviate from that of the pre-UV θ_g's, but in the opposite direction from what would have been expected by the presence of now a more significant level of the polymer substructure. This is because in a post-UV

electrolyte of any w value, the $\theta_{g,s}$, when measurable, only reflects the glass transition of the solution substructure, and the creation of the polymer substructure by the UV irradiation makes the remaining solution substructure less viscous by extricating PDA monomers from it. As w further rises, the polymer substructure eventually builds up to such a level that its $\theta_{g,p}$ becomes measurable, and the second branch of $\theta_{g,p}$ comes into view and so begins the double glass transition region. This region ends when the signals for $\theta_{g,s}$ become too weak to measure, and, with only $\theta_{g,p}$ measurable, the polymer-dominant region begins.

The same reasoning explains the $\theta_{0,s}$ curve dropping below the θ_0 curve upon UV irradiation, as shown in Figure 8 with the blue and green triangles. Despite the existence of the nonconducting polymer substructure in a post-UV electrolyte, the lower effective value of w in the solution substructure lowers its viscosity and thereby allows the κ of the post-UV electrolyte to decline more slowly with a falling θ than its pre-UV counterpart, especially at lower temperatures, resulting in a lower $\theta_{0,s}$. This lower effective w also contributes to the reductions in the rate of decline with w in both θ_l and θ_s, as are also shown in the figure. In contrast, the storage modulus of the gel material is dominated solely by its polymer substructure; thus, it increases rapidly with w as more polymer substructure is built up. The dependency of g_κ on w, on the other hand, is largely dictated by that of the solution substructure; therefore, for the lower part of w's, the UV irradiation promotes the κ by reducing the effective w of the solution substructure thus making g_κ positive or limiting it to only mildly negative values. As the w further rises, however, the irradiation leaves too little solution substructure to carry the ionic currents and makes too much polymer substructure blocking the passageways for these currents, thus resulting in the quick falls in the g_κ curves.

4. Conclusions

We have characterized and studied a system of polymer-supported aqueous electrolytes, wPDA + (1–w)LiTFSI$_{12m}$H$_2$O, where the starting materials were all in the liquid state and the polymerized materials via UV irradiation could be in the state of liquid, gel, or solid, depending on the value of w. All the compositions, both pre- and post-UV, were characterized selectively with thermoconductometry, rheometry, and glass transition analysis. The polymerization of a starting liquid generated in it a polymer substructure of PDA and a solution substructure of an altered composition, the two substructures mutually soluble but distinct from each other. The distinction was manifested in the transformation of a single track of glass transition temperatures, $\theta_g(w)$, of the starting compositions into a double track of $\theta_{g,s}(w)$–$\theta_{g,p}(w)$ of the solution and polymer substructures of the post-UV materials, with the gels displaying both tracks simultaneously. The strong thermal signals of

the double glass transitions in the present electrolyte system enabled the accurate determination of the gel range by the extrapolation of the height of their heat flow steps. Separately, the polymer substructure in the gel electrolyte gave it a storage modulus that rose rapidly with *w*, and the solution substructure, an exceptional conductivity. This exception could be seen in the conductivity gains upon polymerization exhibited by many of the gel compositions, and in their values being more than 2 orders of magnitude higher than some typical true polymer electrolytes. The alteration of the composition of the solution substructure by polymerization also resulted in the vanishing conductivity temperatures of the gel electrolytes dropping below those of their precursors, and in a reduction in the decline of the liquidus points with *w*. The combination of high rigidities in the gel electrolytes and their unusually high conductivities, resulting from the coexisting polymer and solution substructures, holds great interest and promise for future electrolyte development.

5. References

1. Ding MS, Cresce AV, Eidson N, Xu K. Polymer-supported aqueous electrolytes for lithium ion batteries: I. Application of a thermoconductometric method to a LiTFSI + H_2O + PDA electrolyte system. J Electrochem Soc. 2022;169:110525.
2. Ding MS, Cresce AV, Eidson N, Xu K. Polymer-supported aqueous electrolytes for lithium ion batteries: II. Conductivity gain upon polymerization and double glass transition in LiTFSI + H_2O + PDA gels. J Electrochem Soc. 2022;169:120524.
3. Ding MS, Xu K. A thermoconductometric study of transient behavior of liquid electrolytes at phase transition. J Phys Chem C. 2021;125:23029.
4. Chen T. Exploring the viscoelastic properties of cheese using a rheometer. TA Instruments Applications Notes, RH098 [date unknown].
5. Novak M. Non-linear oscillation testing of viscoelastic fluids. TA Instruments Applications Notes, ANN113 [date unknown].
6. Zhang J et al. Safety-reinforced poly(propylene carbonate)-based all-solid-state polymer electrolyte for ambient-temperature solid polymer lithium batteries. Adv Energy Mater. 2015;5:1501082.
7. Nguyen PT, Snyder JF. Multifunctional properties of structural gel electrolytes. Army Research Laboratory (US); 2008. Report No.: ARL-RP-223.
8. Shin JH, Passerini S. PEO-LiN($SO_2CF_2CF_3$)$_2$ polymer electrolytes – V. Effect of fillers on ionic transport properties. J Electrochem Soc. 2004;151:A238.
9. Villano P, Carewska M, Appetecchi GB, Passerini S. PEO-LiN($SO_2CF_2CF_3$)$_2$ polymer electrolytes – III. Test in batteries. J Electrochem Soc. 2002;149:A1282.
10. Song JY, Wang YY, Wan C. Review of gel-type polymer electrolytes for lithium-ion batteries. J Power Sources 1999;77:183−197.
11. Peled E, Golodnitsky D, Ardel G. Advanced model for solid electrolyte interphase electrodes in liquid and polymer electrolytes. J Electrochem Soc. 1997;144:L208−L210.
12. Koksbang R, Olsen II, Shackle D. Review of hybrid polymer electrolytes and rechargeable lithium batteries. Solid State Ion. 1994;69(3−4):320−335.

13. Boden N, Leng SA, Ward IM. Ionic conductivity and diffusivity in polyethylene oxide/electrolyte solutions as models for polymer electrolytes. Solid State Ion. 1991;45:261−270.

14. Fenton DE, Parker JM, Wright PV. Complexes of alkali metal ions with poly(ethylene oxide). Polymer. 1973;14:589.

15. Ferry JD. Viscoelastic properties of polymers. 3rd ed. John Wiley & Sons; 1980. Chapter 17.

16. Fergus JW. Ceramic and polymeric solid electrolytes for lithium-ion batteries. J Power Sources. 2010;195:4554–4569.

17. Wang S-H, Hou S-S, Kuo P-L, Teng H. Poly(ethylene oxide)-co-poly(propylene oxide)-based gel electrolyte with high ionic conductivity and mechanical integrity for lithium-ion batteries. ACS Appl Mater Interfaces. 2013;5:8477–8485.

18. Devaux D, Bouchet R, Glé D, Denoyel R. Mechanism of ion transport in PEO/LiTFSI complexes: Effect of temperature, molecular weight and end groups. Solid State Ion. 2012;227:119–127.

19. Shin J-H, Henderson WA, Passerini S. An elegant fix for polymer electrolytes. Electrochem Solid-State Lett. 2005;8:A125.

20. Cresce A et al. Gel electrolyte for a 4V flexible aqueous lithium-ion battery. J Power Sources. 2020;469:228378.

21. Angell CA. Formation of glasses from liquids and biopolymers. Science. 1995;267:1924−1935.

22. Cassel RB. How Tzero technology improves DSC performance, part III: the measurement of specific heat capacity. TA Instruments Applications Notes, TA297 [date unknown].

23. Ding MS, Xu K. Phase diagram, conductivity, and glass transition of LiTFSI–H_2O binary electrolytes. J Phys Chem C. 2018;122:16624−16629.

24. Tominaga Y. Ion-conducting polymer electrolytes based on poly(ethylene carbonate) and its derivatives. Polymer J. 2017;49:291–299.

25. Ding MS, Jow TR. Conductivity and viscosity of PC-DEC and PC-EC solutions of $LiPF_6$. J Electrochem Soc. 2003;150:A620–A628.

26. Ding MS. Conductivity and viscosity of PC-DEC and PC-EC solutions of $LiBF_4$. J Electrochem Soc. 2004;151:A40–A47.

27. Smedley SI. The interpretation of ionic conductivity in liquids. Plenum Press; 1980. Chapter 3.

28. Xu W, Angell CA. LiBOB and its derivatives: weakly coordinating anions, and the exceptional conductivity of their nonaqeous solutions. Electrochem Solid-State Lett. 2001;4:E1−E4.

29. Ding MS. Liquid-solid phase diagrams of ternary and quaternary organic carbonates. J Electrochem Soc. 2004;151:A731–A738.

30. Ding MS. Thermodynamic analysis of phase diagrams of binary carbonates based on a regular solution model. J Electrochem Soc. 2002;149:A1063–A1068.

List of Symbols, Abbreviations, and Acronyms

C_p	specific heat capacity at constant pressure
$C_{p,p}$	specific heat capacity in a gel due to its polymer substructure
$C_{p,s}$	specific heat capacity in a gel due to its solution substructure
E_a	activation energy
G'	storage modulus
g_κ	conductivity gain upon polymerization
κ	electrolytic conductivity
R	the gas constant
T	temperature in kelvin
T_0	vanishing conductivity temperature in kelvin
T_g	glass transition temperature in kelvin
θ	temperature in Celsius
θ_g	glass transition temperature in Celsius
$\theta_{g,p}$	glass transition temperature in a gel due to its polymer substructure
$\theta_{g,s}$	glass transition temperature in a gel due to its solution substructure
θ_0	vanishing conductivity temperature in Celsius
$\theta_{0,s}$	vanishing conductivity temperature in a gel due to its solution substructure
θ_l	liquidus temperature of a solution
θ_s	solidus temperature of a solution
w	concentration in weight fraction
DSC	differential scanning calorimetry/calorimeter
LiTFSI	lithium bis(trifluoromethanesulfonyl)imide
PC	personal computer
PDA	poly(ethylene glycol) diacrylate
UV	ultraviolet
VFT	Vogel−Fulcher−Tammann

1 (PDF)	DEFENSE TECHNICAL INFORMATION CTR DTIC OCA
1 (PDF)	DEVCOM ARL FCDD RLB CI TECH LIB